The EMBO Journal vol.8 no.5 pp.1567 - 1579, 1989

Structural factors that control conformational transitions and serotype specificity in type 3 poliovirus

David J.Filman, Rashid Syed, Marie Chow[1], Andrew J.Macadam[2], Philip D.Minor[2] and James M.Hogle

Department of Molecular Biology, Research Institute of Scripps Clinic, 10666 North Torrey Pines Road, La Jolla, CA 92037, [1]Department of Biology, Massachusetts Institute of Technology, Cambridge, MA 02139, USA and [2]National Institute for Biological Standards and Control, Blanche Lane, Potters Bar, Hertfordshire EN6 3QG, UK

Communicated by J.Skehel

The three-dimensional structure of the Sabin strain of type 3 poliovirus has been determined at 2.4 Å resolution. Significant structural differences with the Mahoney strain of type 1 poliovirus are confined to loops and terminal extensions of the capsid proteins, occur in all of the major antigenic sites of the virion and typically involve insertions, deletions or the replacement of prolines. Several newly identified components of the structure participate in assembly-dependent interactions which are relevant to the biologically important processes of viral assembly and uncoating. These include two sites of lipid substitution, two putative nucleotides and a beta sheet formed by the N-termini of capsid proteins VP4 and VP1. The structure provides an explanation for the temperature sensitive phenotype of the P3/Sabin strain. Amino acids that regulate temperature sensitivity in type 3 poliovirus are located in the interfaces between promoters, in the binding site for a lipid substituent and in an assembly-dependent extended beta sheet that stabilizes the association of pentamers. Several lines of evidence indicate that these structural components also control conformational transitions at various stages of the viral life cycle.

Key words: poliovirus structure/picornavirus structure/thermo-stability/serotype specificity/conformational rearrangements

Introduction

The polioviruses include a number of related strains which are the causative agents of poliomyelitis in man. Like other members of the picornavirus family (coxsackie-, rhino-, cardioviruses, foot and mouth disease and hepatitis A viruses), the polioviruses are nonenveloped icosahedral viruses. Each virion contains one copy of a single-stranded messenger-sense RNA genome enclosed in a roughly spherical capsid which is ~310 Å in diameter. The capsid is composed of 60 copies of each of four coat protein subunits, VP1 (33 kd), VP2 (30 kd), VP3 (26 kd) and VP4 (7.4 kd), arranged on a $T = 1$ icosahedral surface. All poliovirus proteins are derived from a large polyprotein (220 kd) by post-translational processing catalyzed by virally encoded proteases. Early in assembly, cleavage of the capsid protein precursor P1 (94 kd) to yield VP0, VP1 and VP3 is associated with the formation of pentameric assembly intermediates. Late in assembly, after the encapsidation of the viral RNA, the cleavage of VP0 to yield VP4 and VP2 completes the assembly process and appears to contribute substantially to the stability of the mature virion (for review see Rueckert, 1985).

All isolates of poliovirus can be assigned to one of three serotypes using panels of reference antisera. In 1985 we reported the structure of the neurovirulent Mahoney strain of type 1 poliovirus (P1/Mahoney) (Hogle *et al.*, 1985). This structure, together with the structures of rhinovirus 14 (Rossmann *et al.*, 1985) and Mengo virus (Luo *et al.*, 1987), has provided considerable insight into picornavirus architecture, evolution, assembly and immune recognition. In this paper we report the structure of the Sabin attenuated vaccine strain of type 3 poliovirus (P3/Sabin), determined at 2.4 Å resolution.

P3/Sabin differs from its neurovirulent parent strain P3/Leon by only 10 nucleotides in the 7500-nucleotide genome. Only two of these differences, a mutation in the 5′ noncoding region of the genome and the substitution of Phe for Ser at position 91 of the capsid protein VP3, contribute significantly to its attenuation (Westrop *et al.*, 1986). The latter substitution is also responsible for the temperature sensitive (ts) phenotype of P3/Sabin, which grows well at 35°C but not at 40°C (Westrop *et al.*, 1986; Minor *et al.*, 1989). A number of second-site mutations that suppress the ts phenotype have been characterized (Minor *et al.*, 1989). The structural role of Phe-91 of VP3 and the locations of the second-site suppressor mutations have suggested a plausible explanation for the ts phenotype and its relationship to thermostability.

Comparison of the P3/Sabin and P1/Mahoney models has provided the first detailed view of the structural differences between serotypes of related spherical viruses. The high degree of sequence homology between the two strains (83%) permits the observed conformational differences to be correlated with specific sequence changes. These correlations will serve as a starting point for future efforts to computationally model the loop structures in polio and closely related viruses. In addition, the availability of two independently derived maps has made it possible to interpret several weak but consistent electron density features. This has allowed the identification of a partially ordered polypeptide segment from the N-terminus of VP1, two sites of lipid substitution and two ordered nucleotides on the inner surface of the capsid. Together, these observations and the locations of ts-regulating mutations provide significant insights into the structural components which regulate virion stability and participate in the biologically important conformational rearrangements that are associated with maturation and cell entry in picornaviruses.

Results

P3/Sabin crystallizes in the orthorhombic space group I222 with $a = 320$, $b = 358$ and $c = 381$ Å. The crystals contain 1/4 virus particle per asymmetric unit and thus express 15-fold noncrystallographic redundancy. Three-dimensional X-ray diffraction data were collected at −15°C by oscillation photography. The three-dimensional data are nearly complete to 3.0 Å resolution and are well sampled with respect to the icosahedrally unique data to 2.4 Å resolution. Statistics for the data are presented in Tables I and II. The structure was solved by molecular replacement using an appropriately oriented, refined model of P1/Mahoney to obtain initial phase estimates. Phases were refined by applying the constraints which are imposed by 15-fold non-crystallographic symmetry. The resulting electron density map provided clear indications for the substitution and deletions which distinguish P3/Sabin and P1/Mahoney. Areas of significant discrepancy between the two structures have been verified by the calculation of icosahedrally constrained 'omit' maps. A complete atomic model for P3/Sabin has been constructed to fit the map and refined by alternating the application of noncrystallographic symmetry constraints, interactive model rebuilding, and stereochemically constrained pseudo-real space refinement (D.J.Filman and J.M.Hogle, in preparation). A similar strategy has been used to refine the structure of P1/Mahoney. Statistics for the current refined atomic models are summarized in Table II.

Table I. Statistics for the P3/Sabin data set

Films (no.)	92
Measurements (no.)	1 661 152
Unique hkl measured (no.)	549 626
Unique hkl used (no.)	520 979
R_{sym} (all measurements)	0.128
R_{sym} (fully recorded reflections)	0.094

R_{sym} compares multiply-measured individual partially corrected intensities (I_{hj}) with their sigma-weighted mean $<I_h>$.

$$R_{sym} = \frac{\sum_h \sum_j | I_{hj} - <I_h> |}{\sum_h \sum_j <I_h>}$$

Overview of the P3/Sabin structure

Consistent with our previous description of the P1/Mahoney structure (Hogle *et al.*, 1985), the capsid proteins VP1, VP2 and VP3 of P3/Sabin have similar conserved cores (eight-stranded antiparallel beta barrels shaped like triangular wedges), dissimilar extensions at their N- and C-termini and

Table II. Statistics for the current atomic models

P3/Sabin						P1/Mahoney					
Resol. no. (Å)[a]	Unique hkl used[b]	% of total shell	R_1 model[c]	R_1 non-x symm.[d]	R_{corr} non-x symm.[e]	Resol. no. (Å)	Unique hkl used[b]	% of total shell	R_1 model[c]	R_1 non-x symm.[d]	R_{corr} non-x symm.[e]
∞-9.60	10411	76.0	0.4153	0.1423	0.9421	∞-11.51	12867	79.5	0.4667	0.1296	0.9521
6.78	20434	82.9	0.3064	0.1217	0.9612	8.14	24806	86.4	0.2359	0.0873	0.9805
5.54	27087	85.7	0.2689	0.1185	0.9631	6.65	32092	87.2	0.2196	0.0964	0.9741
4.80	32756	87.8	0.2235	0.1074	0.9688	5.76	37870	87.3	0.1719	0.0925	0.9748
4.29	37635	89.0	0.1972	0.1058	0.9690	5.15	42699	87.0	0.1539	0.0912	0.9746
3.92	41991	90.0	0.1994	0.1170	0.9634	4.70	47022	86.9	0.1352	0.0885	0.9754
3.63	46001	90.9	0.2118	0.1248	0.9602	4.35	50655	86.2	0.1328	0.0918	0.9727
3.39	49651	91.4	0.2303	0.1390	0.9528	4.07	53343	84.6	0.1432	0.0972	0.9685
3.20	52832	91.5	0.2562	0.1530	0.9447	3.84	55460	82.8	0.1482	0.1037	0.9638
3.03	54180	88.7	0.2985	0.1768	0.9306	3.64	57445	81.1	0.1571	0.1083	0.9595
2.89	45764	71.4	0.3316	0.2085	0.9050	3.47	56615	76.1	0.1707	0.1205	0.9476
2.77	36263	54.1	0.3775	0.2501	0.8737	3.32	56267	72.3	0.1808	0.1287	0.9374
2.66	27221	38.9	0.4140	0.2857	0.8462	3.19	54805	67.6	0.1903	0.1372	0.9272
2.56	20301	28.0	0.4530	0.3359	0.7960	3.08	51497	61.2	0.2084	0.1492	0.9120
2.48	14028	18.7	0.4963	0.3776	0.7567	2.97	44614	51.1	0.2285	0.1674	0.8893
2.40	4424	5.8	0.5150	0.4054	0.7189	2.88	34560	39.0	0.2505	0.2166	0.8238
total	520979	61.6	0.2677	0.1544	0.9535	total	712617	72.6	0.1773	0.1345	0.9577

The current atomic models for P3/Sabin and P1/Mahoney include, respectively, 6653 and 6690 non-hydrogen atoms, representing the protein, myristate, and sphingosine in each protomer, and 405 and 479 fixed solvent molecules with variable individual occupancy factors. Both models have a 0.04 Å rms deviation of the atomic positions from rigidly constrained standard groups, and a 0.02 Å rms deviation from standard bond lengths. The P1/Mahoney (but not the P3/Sabin) model includes restrained individual isotropic temperature factors.

R_1 and R_{corr} (the linear correlation coefficient) are measures of the agreement between two sets of structure factor amplitudes: those observed and those calculated by Fourier inversion of either (c) the atomic model or (d) (e) the averaged electron density map.

$$R_1 = \frac{\sum_{hkl} ||F_{obsd}| - |F_{calc}||}{\sum_{hkl} |F_{obsd}|}$$

[a]The reflections have been divided into 16 shells of roughly equal reciprocal volume. The values in each shell correspond to: [b]the number of unique reflections in the data set, (%) the percentage of possible reflections which this number represents and [c] R_1, where F_{calc} is the transform of the atomic model. After non-crystallographic symmetry constraints have been applied to model-based phases, the quality of the resulting symmetry-averaged electron density map can be assessed by [d]R_1, where F_{calc} is the Fourier transform of the averaged map and [e]the linear correlation coefficient.

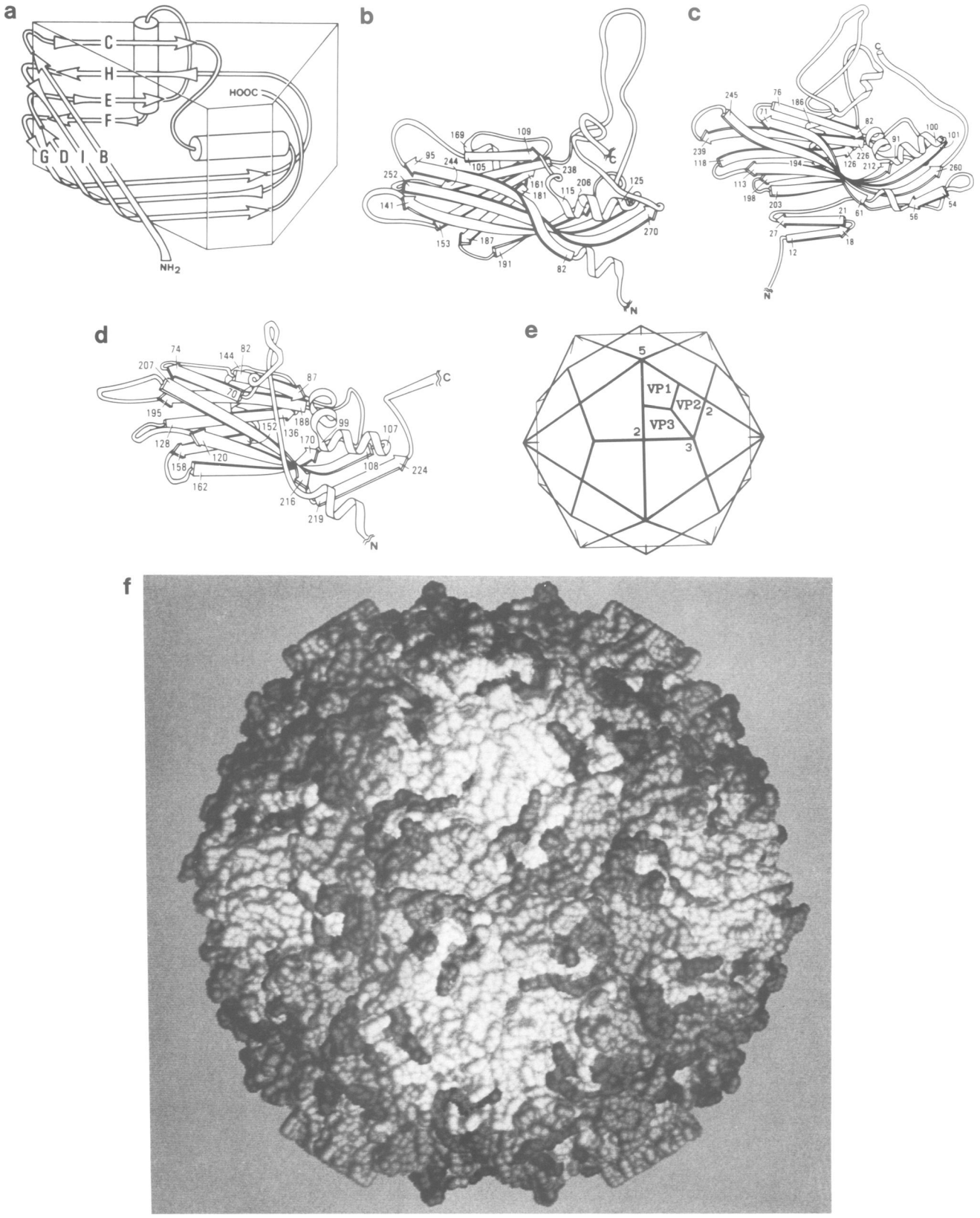

Fig. 1. The structure and organization of the major capsid proteins of poliovirus. (**a**) Schematic representation of the conserved wedge-shaped eight-stranded antiparallel beta barrel core motif shared by VP1, VP2 and VP3. Individual beta strands are shown as arrows and are labeled alphabetically. Flanking helices are indicated by cylinders. (**b**–**d**) Ribbon diagrams of VP1 (b), VP2 (c) and VP3 (d). Residue numbers have been included as landmarks. Extensions at the N- and C-termini of VP1 and VP3 have been truncated for clarity. (**e**) A geometric representation of the outer surface of the poliovirion is generated by superimposing an icosahedron and a dodecahedron. The symmetry axes of the particle and the positions of VP1, VP2 and VP3 in one protomer are indicated. Like the virion, the geometric figure has large radial projections at the 5-fold axes and somewhat smaller projections at the 3-fold axes. (**f**) This space-filling representation of the outer surface is in the same orientation as the geometric figure in (e). In the center of the picture, VP1 is light-gray, VP2 is medium-gray and VP3 is dark-gray. Depth-cueing causes all three proteins to appear darker at the periphery of the view.

dissimilar loops connecting the regular secondary structural elements of the cores (Figure 1a–d). In the virions the cores form a closed protein shell, with the narrow ends of the VP1 beta barrels clustered around the particle 5-fold axes and the narrow ends of the cores of VP2 and VP3 alternating around the particle 3-fold axes (Figure 1e–f). The tilting of the cores outward along these axes produces radial projections at the 5-fold and 3-fold axes, with broad shallow valleys separating the projections. Similar core structures and packing arrangements have been seen in a variety of small RNA viruses, including picornaviruses (Hogle *et al.*, 1985; Rossmann *et al.*, 1985; Luo *et al.*, 1987), several families of plant virus (Harrison *et al.*, 1978; Abad-Zapatero *et al.*, 1980; Liljas *et al.*, 1982; Hogle *et al.*, 1986b; Stauffacher *et al.*, 1987) and an insect virus (Hosur *et al.*, 1988). The C-termini and connecting loops form the major features exposed on the outer surface of the virion, and include most of the residues identified as parts of neutralizing antigenic sites (Minor *et al.*, 1983, 1985, 1986; Diamond *et al.*, 1985; Page *et al.*, 1988). The N-terminal extensions and VP4 form a network on the inner surface of the capsid. The formation of this network depends on the processing of P1 to free the N-termini of VP1 and VP3, which accounts for the coupling of these cleavages to early events in assembly. As discussed below,

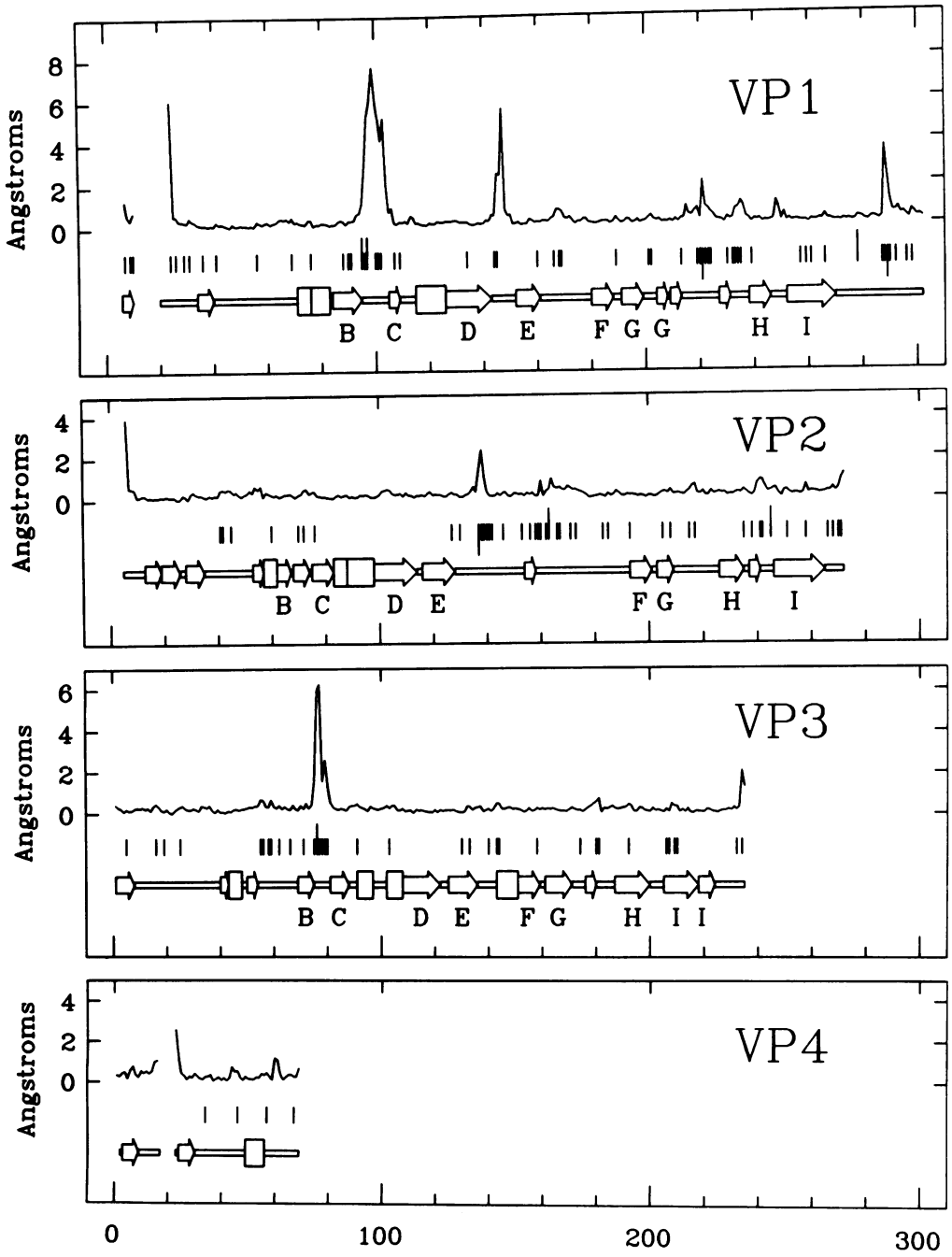

Fig. 2. Comparison between the capsid protein structures of the P3/Sabin and P1/Mahoney strains of poliovirus. At the top of each panel, the difference in position of structurally equivalent alpha carbons is plotted as a function of residue number. The vertical hash marks below each plot indicate differences in amino acid sequence. The larger hash marks extending upward indicate proline replacement, and those extending downward indicate insertions and deletions. At the bottom of each panel, the locations of alpha helices and beta strands are indicated by wide rectangles and by arrows respectively. The eight strands of the antiparallel beta barrel core motif of VP1, VP2 and VP3 are labeled B–I.

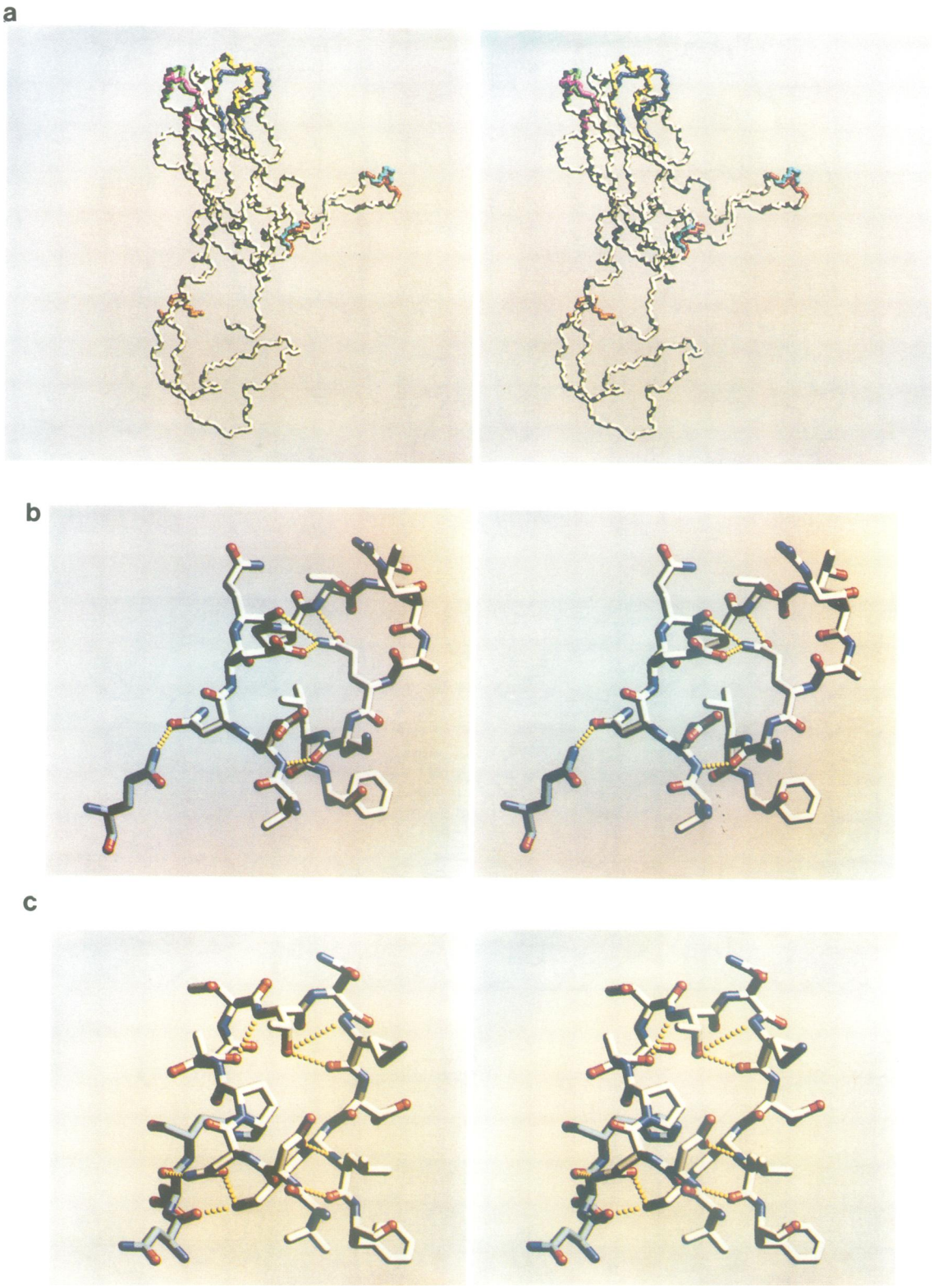

Fig. 3. Significant structural differences in capsid protein VP1 of P3/Sabin and P1/Mahoney. (**a**) In this stereo representation of the main chain conformation, structurally conserved main chain atoms are white. Differences, which are observed only in the loops and terminal extensions of the capsid proteins, are shown in color. The B−C loop (dark blue in P3/Sabin and yellow in P1/Mahoney) involves the replacement of proline residues in a loop having substantial sequence differences. The D−E loops (green in P3/Sabin and magenta in P1/Mahoney) are significantly different in the two structures despite their general similarity in sequence. The highly localized structural changes due to one-residue insertions or deletions are indicated in cyan in P3/Sabin and in red in P1/Mahoney. The residues indicated in orange represent a portion of the amino terminal extension (residues 20−23) which is ordered in P1/Mahoney, but which is disordered in P3/Sabin. Parts (**b**) and (**c**) are stereo pairs showing the atomic structure of the B−C loop in P3/Sabin and P1/Mahoney respectively. Oxygen atoms are red and nitrogens are dark blue. The carbon atoms shown in white belong to the B−C loop, while those shown in light blue belong to adjacent portions of the protein which make structurally important interactions with the loop. The yellow dotted lines represent hydrogen bonds which stabilize the B−C loop and which appear to play significant roles in determining its conformation.

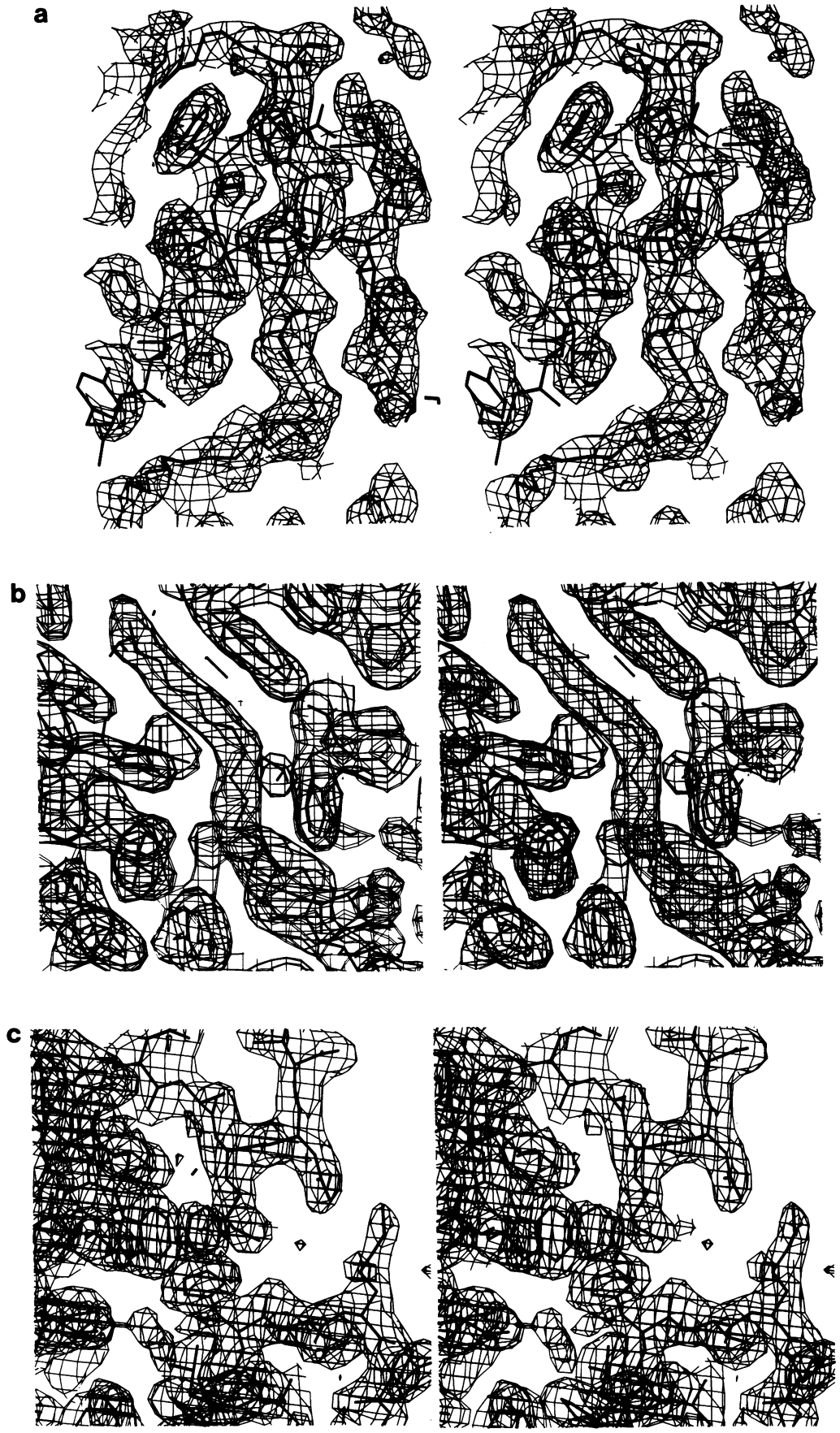
a
b
c

other components of this network may explain the role of VP0 cleavage in the maturation of the virion.

Comparison of the structures of P3/Sabin and P1/Mahoney

P3/Sabin and P1/Mahoney share 83% identity in the amino acid sequence of the capsid proteins. Consistent with this degree of homology, the two structures are strikingly similar. The rms difference in alpha carbon positions is 0.78 Å for 846 sequentially equivalent residues, and the difference is reduced to only 0.34 Å when the 19 pairwise discrepancies >2.0 Å are omitted. As illustrated in Figures 2 and 3a, the structures are remarkably similar throughout the cores of the capsid protein subunits, the N-terminal extensions and many of the connecting loops. Sequence differences in these areas are accommodated through local adjustments of side chain conformation or by compensating changes in neighboring side chains.

Structural conservation in the cores is not surprising because the precise atomic complementarity within and between the beta barrels limits both sequence and structural variability in these residues. The degree of structural conservation in the loops and terminal extensions was less predictable. Because these loops and terminal extensions are not constrained by obvious packing considerations, their structural conservation serves as a likely indication that these residues are involved in the dynamic processes of the virus, e.g. assembly, receptor binding and uncoating.

Significant structural differences occur only in the exposed loops and chain termini of the virus (see Figure 2). These structural differences fall into three general categories. (i) Structural differences in loops due to insertions in one strain relative to the other. The observable insertions occur at residue 221 of VP1 in P3/Sabin, at residue 289 of VP1 in P1/Mahoney and at residue 138 of VP2 in P1/Mahoney. These insertions cause limited, highly localized structural perturbations which have little effect further than one or two residues on either side of the insertion (Figure 3a). (ii) Loops which contain several sequence differences, including the replacement of proline residues. Examples include conformational changes in the B−C loop of VP1 (residues 95−105), the B−C loop of VP3 (residues 75−81) and the H−I loop of VP2 (residues 235−245). The importance of proline replacement is suggested by residues 143−187 in the E−F loop of VP2, which has no proline replacements, and is nearly identical in conformation in the two strains despite numerous sequence differences. (iii) Differences observed at points of transition between ordered and disordered structure (indicated by large discrepancies in alpha carbon positions at gaps and chain termini in Figure 2). These differences may merely represent alternative sampling of weakly ordered structures and are unlikely to be biologically significant.

The structural difference in the D−E loop of VP1 (residues 141−153) does not fall into any of these categories. The explanation for this difference is not straightforward because the sequence of the loop is relative conserved, and neither of the two variable residues (residues 144−145) is involved in obvious stabilizing interactions. The conformational change in this relatively flexible loop may be coupled with the pronounced structural differences in the nearby B−C loop of VP1 (Figure 3a−c).

Additional components of the virion structure

During the interpretation and refinement of the P3/Sabin structure, several electron density features were identified which were not present in the initial phasing model (Figure 4a−c). Although these features are weak, and with one exception have yet to be corroborated by independent chemical evidence, they are considered to be reliable insofar as nearly identical features have been identified in the refined P1/Mahoney map. Two of the newly interpreted features are located in the complex formed by the interaction of five copies of the N-termini of VP3 and VP4 on the inner surface of the capsid at each 5-fold axis (Figure 5a). As we have described previously, the intertwined N-termini of VP3 form a twisted tube of parallel beta structure. This tube is flanked by five copies of a short two-stranded antiparallel beta sheet which is formed by residues 3−8 and 25−29 of VP4. Note that six of the residues that connect the two beta strands (residues 17−22) are entirely disordered.

There is a roughly crescent-shaped electron density feature extending from the N-terminal glycine of VP4 in both the P3/Sabin and P1/Mahoney structures (Figure 4a). The identity of this density was established when radiolabeling experiments showed that the N-terminus of VP4 and its precursors (VP0 and P1) are myristoylated (Chow *et al.*, 1987). The myristate clearly plays an integral role in the capsid structure, mediating the interaction between the N-termini of VP3 and VP4, and shielding the hydrophobic side chains of Leu-2 and Pro-3 of VP3. We also have proposed that the myristate may play a role in directing VP4 or its precursors to membranes during the assembly of the virus or in its entry into the cell (Chow *et al.*, 1987).

Both the P3/Sabin and the refined P1/Mahoney maps also clearly indicate the presence of a third beta strand, five

Fig. 4. Stereo plots of the P3/Sabin electron density map in three regions of particular interest. Electron density contours have been truncated at the front and back of each view for clarity. (**a**) The beta sheet formed by the N-terminus of VP4 is well resolved in the refined poliovirus maps. The myristic acid moiety which is covalently linked to the N-terminal glycine of VP4 (Gly-2) is shown extending across the bottom of the picture, adjacent and roughly parallel to the 5-fold axis of the virus. Electron density for the N-terminal beta strand of VP4 (residues 3−8) runs vertically through the center of the picture. A portion of the density for the other beta strand of VP4 (residues 25−29) is shown at the left. The electron density feature at the right appears to form a third beta strand, and we have tentatively identified it as a portion of the N-terminus of VP1. (**b**) The elongated feature that occupies the center of the VP1 beta barrel. The most deeply buried portion of this unidentified molecule (shown at the upper left) is in contact exclusively with hydrophobic side chains of VP1, suggesting that the molecule is a lipid. The less well-order density at the lower right is in a polar environment close to the surface of the protein. A model for sphingosine, which fits the hydrogen bonding requirements of the site is shown superimposed on the electron density. (**c**) A planar electron density feature believed to correspond to a particularly favorable binding site for nucleotides is stacked with the indole ring of Trp-38 of VP2. A six-membered ring has been superimposed on the planar density at the center of the picture. The binding site appears to be formed by residues from VP2 (on the left of this view), from the carboxyl end of VP4 (at the top right), and from VP1 from a 3-fold-related protomer (at the bottom right). This portion of VP1 participates in forming the assembly-dependent seven-stranded extended beta sheet.

residues long, extending the two-stranded beta sheet of VP4 towards the interior of the virus (Figure 4a). Although the main chain is unmistakably making parallel beta interactions, neither electron density map is as yet sufficiently well resolved in this area to allow for an unambiguous identification of the side chains in this additional beta strand. However, among the residues unaccounted for in the atomic models (residues 1−19 of VP1, 1−4 of VP2, 236−238 of VP3 and 17−22 of VP4) only the first 16 amino acids of VP1 could possibly be in this vicinity. The interaction between the amino termini of VP1 and VP4 has important implications for the mechanism of viral uncoating (discussed below).

In both the P3/Sabin and P1/Mahoney maps, there is a well-resolved elongated electron density feature, bent in the middle, which extends through the hydrophobic interior of the VP1 beta barrel (Figure 4b). This feature can be model-built convincingly as a 16-carbon saturated chain with

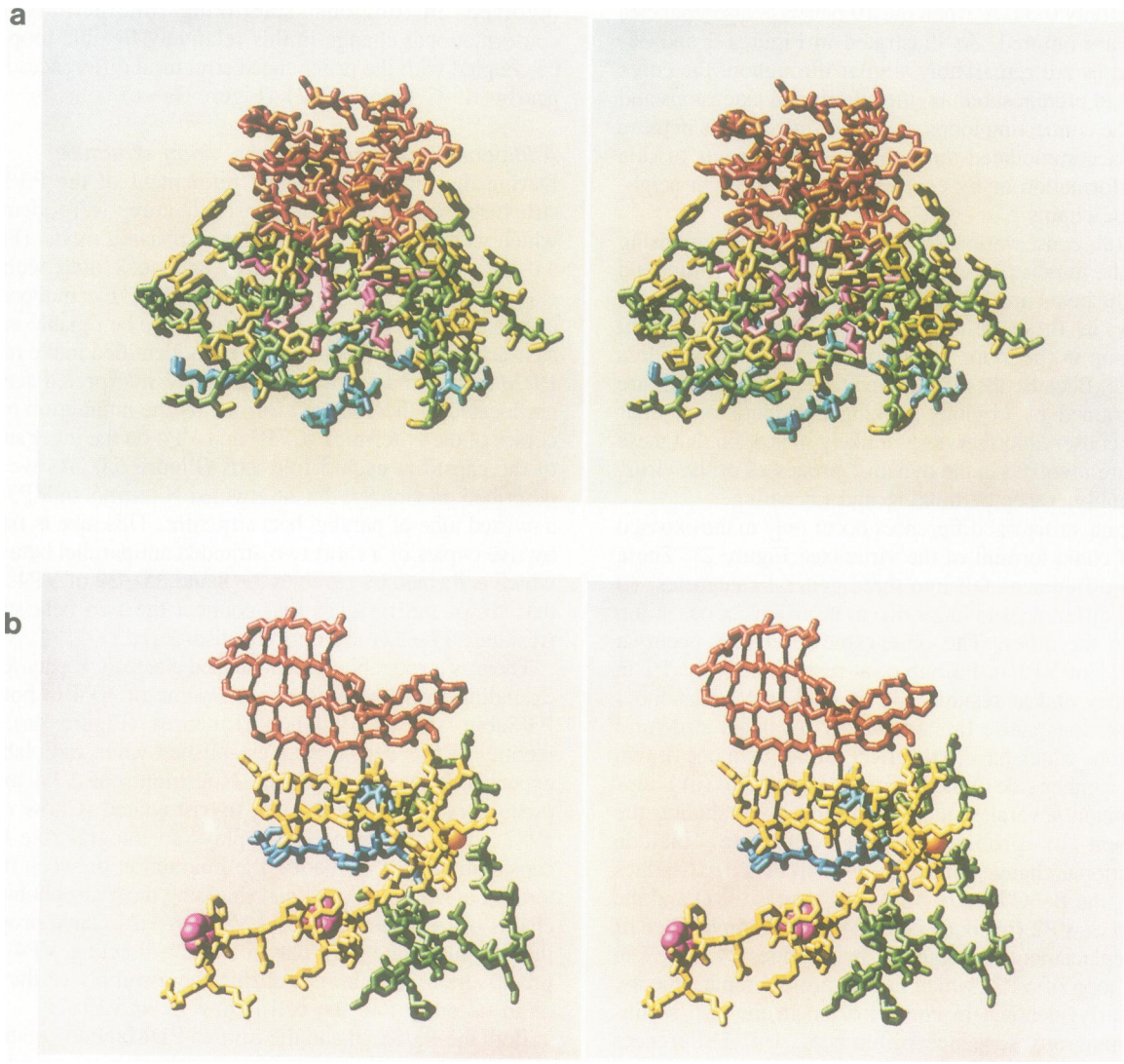

Fig. 5. Assembly-dependent structures which contribute substantially to the stability of the poliovirion. (**a**) The complex formed by the interaction of the N-termini of VP3, VP4 and VP1 around each 5-fold axis appears to be important for directing the assembly of protomers to form pentamers. In this stereo view, the inner surface of the capsid (which is located roughly 90 Å from the center of the particle) is shown at the bottom. The top of the complex is located at a radius of ~130 Å (as compared with the outer surface of the virion, which extends to a radius of 165 Å near the 5-fold axis). At the top of the view, five intertwined N-termini of VP3 (residues 1−11, shown in red) form a twisted tube of parallel beta structure. Five copies of the N-terminus of VP4 (residues 2−8 and 23−33, shown in green with yellow side chains) form short segments of two-stranded antiparallel beta sheet on the inner surface of the capsid. The N-terminal glycine of each copy of VP4 is linked via an amide bond to a myristic acid moiety (shown in magenta). Each of the five-residue segments of polypeptide chain (shown in blue) is believed to be a portion of the N-terminus of VP1. Although the electron density for this chain is consistent with a parallel beta main chain hydrogen bonding pattern, the electron density for the side chains is not sufficiently well resolved to correlate with the capsid sequence of the virus. (**b**) The seven-stranded extended beta sheet which is located near the 3-fold axis of the virion stabilizes the association of neighboring pentamers. In this stereo view, the outer surface of the capsid is at the top and the inner surface of the capsid is at the bottom. Black lines indicate the main chain hydrogen bonds of the extended beta sheet. At the top, the C, H, E and F strands of the VP3 beta barrel (shown in red) form the outermost four strands of the extended sheet. The seventh strand (shown in blue) is formed by residues 36−38 of VP1 from the same protomer. In the foreground, residues from a 3-fold-related protomer are shown. The N-terminal extension of VP2 (yellow) forms the fifth and sixth strands of the beta sheet, interacts with the C-terminus of VP4 (green) and binds two planar electron density features (shown in magenta) which tentatively have been identified as nucleotides of the viral RNA. The large orange sphere represents the side chain hydroxyl group of Ser-10 of VP2. This group is hydrogen bonded to the cleaved carboxyl terminus of VP4 in the mature virion, and may participate in the mechanism of VP0 cleavage. In the background, the C-terminus of VP4 from the first protomer is shown in green.

minimum-energy torsion angles. The 15 most deeply buried atoms in the chain make contact exclusively with hydrophobic side chains of the protein. Beyond the 16th carbon, the electron density for the substituent is discontinuous, and the environment is polar, consistent with a partially ordered polar head group. This end of the substituent is located near the outer surface of the virion, at the base of the G–H loop of VP1. The shape of the electron density and the hydrogen bonding requirements of the polar end are consistent with the provisional identification of the lipid substituent as sphingosine. However, the identity of the substituent has not yet been confirmed by chemical means and we cannot rule out the presence of a mixture of lipids. The hydrocarbon-binding site is nearly identical to the site which binds a class of antiviral drugs in rhinovirus 14 (Smith *et al.*, 1986; Badger *et al.*, 1988).

On the inner surface of the capsid, there are several (mostly uninterpretable) electron density features which may correspond to portions of the disordered RNA genome of the virus. Among these features, however, are two particularly convincing, distinctly planar features (Figure 4c) which are observed in both strains of the virus, and which appear to be stacked with the aromatic side chains of Trp-38 and Phe-41 of VP2 (Trp-38 and Tyr-41 in P1/Mahoney) (Figure 5b). Because all of the aromatic residues of the capsid proteins have been accounted for, we have tentatively identified the planar density features as nucleotide bases. A similar electron density feature, stacked with the structurally analogous Trp-38 of VP2, also has been identified as a nucleotide base in rhinovirus 14 (Arnold and Rossmann, 1988). The apparent conservation of nucleotide binding sites in three different picornavirus structures provides strong evidence for their biological importance. A specific role for these sites in the assembly and maturation of virions is suggested by their locations, as discussed below.

Discussion

Serotype-specific conformations of antigenic loops

Significant conformational differences between P3/Sabin and P1/Mahoney occur only in the exposed loops of the capsid proteins, most often at the sites of insertions, deletions or the replacement of proline residues in loops with several sequence changes. Significant conformational differences have been observed in each of the three major antigenic sites of the virion [as defined by Page *et al.* (1988)]. Thus, structural changes are seen in the B–C loop of VP1 (which constitutes a major portion of antigenic site 1), the B–C loop of VP3 (site 3B), the insertion at residue 221 in the G–H loop of VP1 (site 2) and the insertion at residue 289 of VP1 (site 3A). This correlation implies that three-dimensional structural differences, as well as simple sequence changes, are important determinants of serotype specificity.

The largest conformational difference between P3/Sabin and P1/Mahoney occurs in the B–C loop of VP1, where the difference between equivalent alpha carbon positions is as large as 8 Å. The loop is considerably more exposed in P3/Sabin. Greater accessibility may be partly responsible for the immunodominance of this antigenic site in serotypes 2 and 3 (but not in type 1) (Icenogle *et al.*, 1986; Minor *et al.*, 1986). However, other factors, including the strain and species of animal immunized, and possibly the route of immunization, modulate the immunodominance of this site in type 3 poliovirus (Icenogle *et al.*, 1986). Interest in this loop has been considerably heightened by the recent construction of viable hybrids in which the B–C loop in type 1 poliovirus has been replaced by the corresponding sequence from type 2 or type 3 (Burke *et al.*, 1988; Martin *et al.*, 1988; Murray *et al.*, 1988a,b). Remarkably, a 10-residue loop from the mouse-adapted P2/Lansing strain was sufficient to permit the normally primate-specific P1/Mahoney strain to cause paralysis in mice (Martin *et al.*, 1988; Murray *et al.*, 1988a) demonstrating that the loop has a pronounced effect on the host range of poliovirus.

The biological importance of the B–C loop has prompted considerable interest in the possibility that this and other loops in poliovirus and related viruses can be modeled computationally. As a first approximation to these modeling studies, we have attempted to identify specific conserved amino acids which contribute to the stability of the B–C loop and which may serve as 'signatures' of serotype-specific loop conformations. A similar approach has been used to predict the structures of complementarity-determining loops in the Fab fragments of antibodies (Chothia *et al.*, 1986; Chothia and Lesk, 1987).

Of the six sequence differences in the B–C loop, the most obvious causes of the conformational difference are the substitution of Glu (P3/Sabin) for Pro (P1/Mahoney) at position 95, the substitution of Pro (P3/Sabin) for Ser (P1/Mahoney) at position 97, and the substitution of Gln (P3/Sabin) for Asp (P1/Mahoney) at position 102. In P3/Sabin the loop conformation is stabilized by several specific interactions (see Figure 3b). The most striking interactions involve the side chain of Gln-102, which extends across the loop to hydrogen bond to the side chain of Glu-95, to the main chain carbonyl oxygen of Gln-96, and to the amide nitrogen of Thr-98. The positions of the latter two main chain atoms are highly constrained by the proline residue (Pro-97) between them. It is interesting that the carboxyl end of the loop has a different conformation in the two strains despite the conservation of Lys-103, Leu-104 and Phe-105. In P3/Sabin, Pro-97 makes favorable hydrophobic interactions with the side chain of Leu-104, while the carboxylate of Glu-95 contributes to the neutralization of the positive charge of Lys-103. Gln-102, Glu-95 and Pro-97 are highly conserved in the known type 3 sequences (Minor *et al.*, 1987).

For comparison, the principal stabilizing interactions of the B–C loop of P1/Mahoney are shown in Figure 3c. The effort to identify a conformational 'signature' for the B–C loop in type 1 poliovirus, however, is more complex because its principal stabilizing interactions (e.g. the bèta turn between residues 96 and 99, the main chain constraints imposed by the proline at residue 95, and the hydrogen bonds to main chain atoms made by the side chains of Thr-99 and Lys-103) are sequence independent, involve residues which are not conserved in type 1 polioviruses, or involve residues which are conserved in all three serotypes. The 'signature' of the type 1 conformation might simply be the absence of a proline at position 97, together with the inability of residues 95 and 102 to form a hydrogen bond across the B–C loop.

Temperature sensitivity in the P3/Sabin strain

The temperature sensitivity of P3/Sabin is due to the presence of phenylalanine at amino acid 91 of VP3 (Westrop *et al.*, 1986; Minor *et al.*, 1989). In both the P3/Sabin and the P1/Mahoney structures residue 91 of VP3 is located in a turn of helix at the carboxyl end of the C strand of the beta

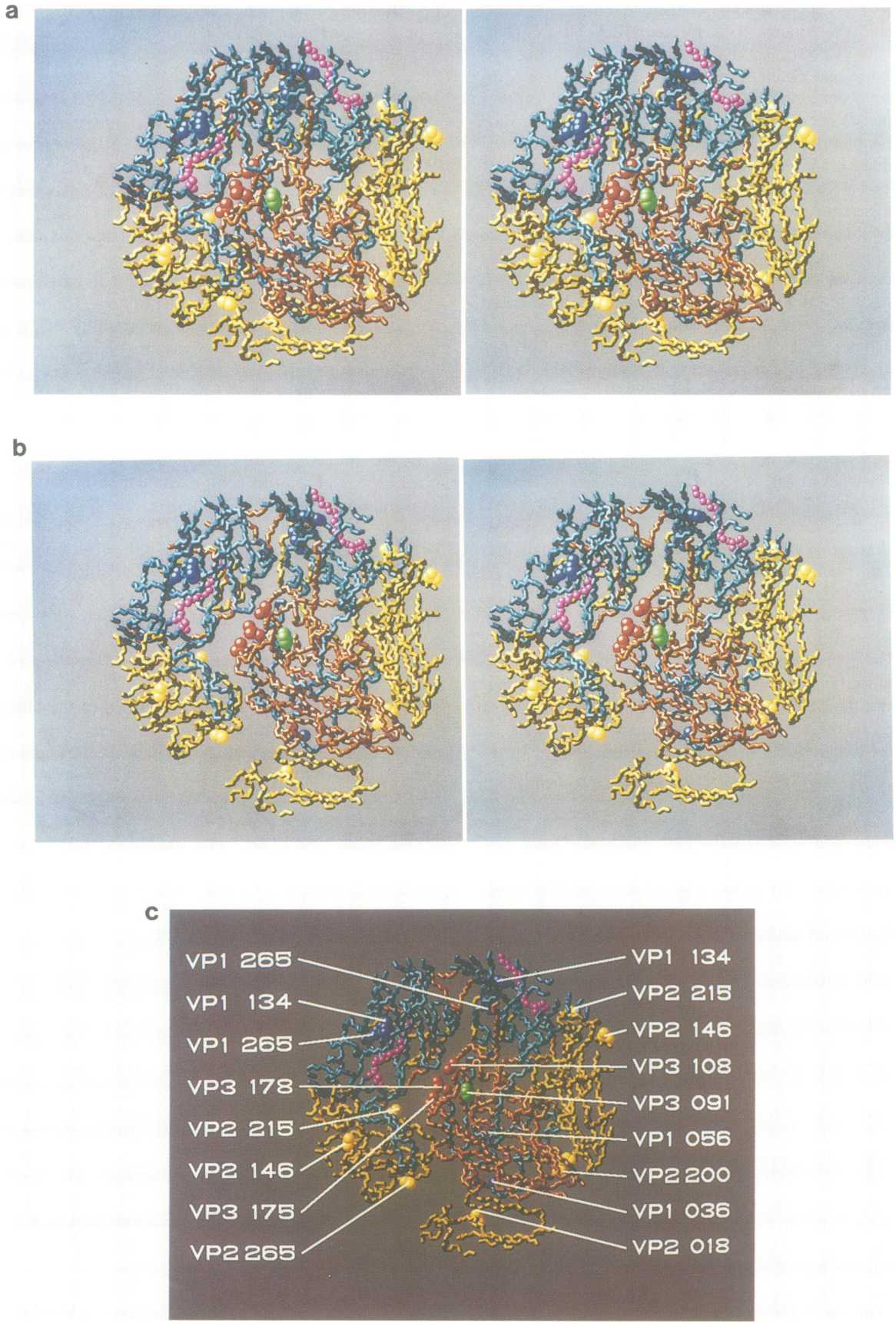
a
b
c
VP1 265
VP1 134
VP1 265
VP3 178
VP2 215
VP2 146
VP3 175
VP2 265
VP1 134
VP2 215
VP2 146
VP3 108
VP3 091
VP1 056
VP2 200
VP1 036
VP2 018

barrel. The G–H loop of VP3 folds across this turn of helix, trapping a chain of three buried solvent molecules in a pocket. In P1/Mahoney, and presumably in P3/Leon (the non-ts parent of P3/Sabin), the side chain of Ser-91 points inward into this pocket and hydrogen bonds to one of the trapped water molecules. In P3/Sabin, however, the side chain of Phe-91 points outward and is fully exposed to solvent at the bottom of the deep valley which surrounds the 5-fold axes of the particle. Indeed, the P3/Sabin electron density maps have clear indications for several ordered solvent molecules adjacent to the edge and to one of the faces of the aromatic side chain. Because solvation of this side chain is energetically unfavorable, we postulate that the substitution of Phe for Ser causes an increased temperature sensitivity in P3/Sabin by affecting the thermostability of the virus particle at some stage of its life cycle. Specifically, the presence of Phe is expected to stabilize conformational states in which the aromatic side chain is buried, and destabilize states in which it is exposed. It is not yet clear whether the effect on thermostability is expressed at the level of the intact virion or whether it affects the dynamic processes of virus assembly and cell entry.

The regulation of structural transitions in poliovirus

A number of non-ts revertants of P3/Sabin have been shown to contain second-site mutations in the capsid proteins (Minor *et al.*, 1989). The majority of these mutations are located in the interfaces between protomers (Figure 6). This suggests that the second-site mutations restore a non-ts phenotype by stabilizing those interfaces which are altered during thermally induced conformational rearrangements. The second-site suppressor mutations which have been characterized to date occur in three general locations: (i) in the interface between 5-fold-related protomers, close to the position of Phe-91; (ii) in the hydrocarbon-binding pocket of VP1; and (iii) in an assembly-dependent beta sheet that stabilizes the association of 3-fold-related pentamers.

Several lines of evidence, discussed below, suggest that modulation of the stability of the interfaces between protomers (and in particular the interface shared by 5-fold-related protomers) may be a common mechanism for the control of structural transitions in picornaviruses during thermal inactivation, viral assembly and uncoating. This model is consistent with the observed distribution of second-site mutations; it explains the ability of molecules occupying the hydrocarbon binding site (including antiviral drugs) to regulate structural transitions; and it predicts an uncoating mechanism which parallels the expansion of plant viruses.

A majority of non-ts revertants have mutations in residues which are located in the interface between 5-fold-related protomers, close to the position of Phe-91 (Figure 6). The involvement of this interface in biologically relevant conformational transitions of the virus is suggested by an analogy with the structurally similar $T = 3$ plant viruses (e.g. tomato bushy stunt virus and turnip crinkle virus). In these plant viruses, the corresponding interface is disrupted during the expansion of the particle which is induced by the depletion of divalent cations at basic pH (Robinson and Harrison, 1982). Upon expansion, portions of the (normally internal) N-termini of the A and B capsid protein subunits are extruded through the disrupted interface (Robinson and Harrison, 1982; Golden and Harrison, 1982). Consistent with the analogy, many of the loops containing second-site mutations in poliovirus correspond to loops in the plant viruses which control expansion by participating in the binding of divalent cations.

The analogy with the expansion of plant viruses may be particularly relevant to a conformational rearrangement in picornaviruses which occurs upon attachment to susceptible cells and results in the loss of the internal protein VP4 from the particle (for review see Rueckert, 1985). We recently have shown that this rearrangement also causes the (normally internal) N-terminus of VP1 to be extruded, and that the exposed N-terminus of VP1 enables the altered particles to attach to liposomes (Fricks, 1988). The exposed N-terminus, together with the myristoylated VP4, may thus participate directly in membrane attachment during cell entry.

In poliovirus, the junction between the beta barrel core and the N-terminal extension of VP1, as well as substantial portions of VP4, lies immediately below the interface which contains the cluster of non-ts mutations. The analogy with the plant viruses would suggest that this interface is disrupted during the conformational transition and serves as the portal for the extrusion of VP4 and of the N-terminus of VP1. The interaction of the N-termini of VP1 and VP4 which is observed in the vicinity of the 5-fold axis (Figure 4a) would then provide a mechanism for coordinating the externalization of these internal components of the capsid protein.

In the second class of second-site suppressors, Phe-134 of VP1 is replaced by leucine. This mutation has been observed in three of four non-ts revertants of virus produced from a (temperature-sensitive) construct in which the Ser at position 91 of VP3 of P3/Leon was replaced by Phe (Minor *et al.*, 1988). Phe-134 is located in the hydrocarbon-binding pocket of VP1 and interacts directly with the bound lipid molecule. The hydrocarbon-binding site in poliovirus is nearly identical to the site which binds a class of antiviral drugs in rhinovirus 14 (Smith *et al.*, 1986; Badger *et al.*, 1988). Once bound, these compounds prevent a variety of conformational rearrangements of the virus, including those required for productive cell entry, and those associated with thermal inactivation (McSharry *et al.*, 1979). This poses the interesting possibility that the antiviral drugs exploit a site that is normally used to modulate the stability of enteroviruses. Simple model-building experiments indicate that a leucine side chain (substituted for Phe-134) would have

Fig. 6. Mutations observed in non-temperature-sensitive revertants of type 3 poliovirus. Parts (**a**) and (**b**) are stereo representations showing the portion of the P3/Sabin structure which is within 40 Å of Phe-91 of VP3. The virion is viewed from the outside, and is oriented so that a 5-fold axis is at the top, a 3-fold axis is at the bottom right and a 2-fold axis is at the bottom center. Main chain atoms are depicted as thin tubes. Large spheres indicate the atoms of side chains that have been found to mutate in one or more of the revertants. Phe-91 is shown in green; VP1 is blue; VP2 and VP4 are yellow; VP3 is red. The extended hydrocarbon which occupies the center of the VP1 beta barrel is magenta. This view includes atoms from three different protomers. The intact model shown in (**a**) has been expanded in (**b**) to separate the protomers and illustrate the tendency of the mutations to cluster in the interfaces between protomers, or in the hydrocarbon binding site. Individual mutations are identified in (**c**).

a more extensive van der Waals interaction with the hydrocarbon ligand, and presumably would influence the stability of the particle by increasing the binding energy of the ligand.

The structural consequences of lipid binding and their effects on the stability of poliovirus can be inferred by analogy with conformational changes induced by drug binding in rhinovirus. Smith *et al.* (1986) have shown that the binding of the antiviral compound WIN 51711 to rhinovirus 14 causes the movement of several residues at the carboxyl end of the G−H loop of VP1. The movement of these residues, which is forced by steric conflicts between the drug and the loop, makes the loop conformation very similar to that observed in poliovirus. In poliovirus these residues make contact with the G−H loop of VP3, close to the cluster of stabilizing mutations in the protomer interface. The analogy suggests that the occupant of the hydrophobic pocket regulates structural transitions of the virus simply by inducing a localized conformational change that causes additional interactions to be formed in the interface between protomers.

The third class of second-site suppressors is exemplified by a non-ts revertant in which Leu-18 of VP2 is replaced by isoleucine. The mechanism by which this residue modulates the stability of the virus is suggested by its location in a previously undescribed seven-stranded beta sheet (Figure 5b), which is formed by residues from two different pentamers. The outermost four strands of the sheet are contributed by the C, H, E and F strands of the beta barrel of VP3 from one protomer; the fifth and sixth strands belong to the two-stranded beta sheet (residues 14−25) at the N-terminus of VP2 from a neighboring 3-fold-related protomer; and the seventh strand is contributed by residues 36−38 in the N-terminal extension of VP1 from the first protomer. This structure obviously contributes to the stability of the association of pentameric subunits in the capsid. Thus, mutations which affect the stability of the sheet could be expected to modulate the stability of virions.

The seven-stranded beta sheet is formed by components of two different pentamers, and the conformation of the innermost three strands is not sensible in the context of an isolated pentamer. Thus, these three strands must rearrange during the assembly of pentamers into capsids, upon the encapsidation of RNA, or as a consequence of the maturation cleavage of VP0. As shown in Figure 5b, the extended beta sheet is located close to the cleaved C-terminus of VP4, and to both of the proposed nucleotide binding sites. Indeed, His-37 in the seventh strand of the sheet is located <5 Å from one of the presumed nucleotide bases. Crystallographic studies (work in progress) on dissociable native-antigenic poliovirus empty capsids (in which VP0 is uncleaved) indicate that the innermost three strands of the sheet are disordered and/or rearranged relative to the native structure, demonstrating that formation of the seven-stranded sheet is dependent on encapsidation of RNA or on the cleavage of VP0, rather than a simple consequence of assembly. These observations begin to provide a structural basis for resolving the unexplained correlation between the encapsidation of RNA, the cleavage of VP0 and the stability of mature virions.

Conclusion

The molecular structure of P3/Sabin and comparisons with the previously described structure of P1/Mahoney have suggested explanations for serotype specificity, temperature sensitivity and structural transitions in poliovirus. The stability of the poliovirus capsid apparently is influenced by a variety of structural factors designed to balance the need for virion stability with the requirement for conformational rearrangements during cell entry. The relationship between temperature sensitivity and structural transitions in P3/Sabin reinforces the picture of poliovirus as a dynamic particle and furnishes insight into the subtle mechanisms that control these structural transitions. These observations have provided a basis for understanding a variety of biological results and a framework for the design and interpretation of future biological and structural studies.

Materials and methods

Virus propagation

Vero cells were grown to high density (10^7 cells/ml) on microcarrier beads (Cytodex 2, Pharmacia) in 1 l Dulbecco's modified Eagle's medium supplemented with 10% calf serum. The cells were inoculated with a low-passage seed stock prepared from a plaque isolate of P3/Sabin [P3/Leon $12a_1b$ plaque number 411 (Stanway *et al.*, 1983)] at a multiplicity of 10 p.f.u./cell. The infected cells were harvested 7 h after infection and washed twice with PBS. The cells were lysed and the virus was purified by differential centrifugation and CsCl density gradient centrifugation using standard procedures (Baron and Baltimore, 1982). The CsCl banded virus was dialyzed against PBS, pelleted through a cushion of 1 M NaCl, 30% sucrose in PBS, and resuspended at a concentration of ~10 mg/ml in 1 M NaCl in PBS.

Crystallization

The concentrated virus was crystallized by dialysis versus progressively lower concentrations of NaCl in PMC7 buffer (10 mM Pipes, 5 mM $MgCl_2$, 1 mM $CaCl_2$, pH 7.0) at 4°C in microdialysis chambers (Cambridge Repetition Engineers). Crystals appeared at ~0.50 M NaCl. The crystals were equilibrated with PMC7 buffer and transferred to a solution containing 25% ethylene glycol in PMC7 (which serves as a cryoprotectant) and mounted in quartz capillary tubes (Charles Supper, Inc.).

Data collection and processing

Three-dimensional diffraction data were collected at −15°C using CuKα radiation from an Enraf-Nonius GX-18 rotating anode generator operated at 40 kV, 55 ma with a 100 μm focus and Franks mirror optics. A total of 92 0.5°-oscillation photographs were obtained from 45 crystals. Exposure times varied from 3 to 6 h depending on the size of the crystal. Photographs were digitized on a 50 μm raster using an Optronics P1000 film scanner and were oriented, integrated by profile-fitting, scaled and post-refined (Winkler *et al.*, 1979) using locally developed software. In constructing the P3/Sabin data set, partially observed reflections ($\geq 50\%$) were corrected to their fully recorded equivalents, partials observed to $<50\%$ were discarded, and a conservative cut based on the intensity and its standard deviation was applied to exclude poorly measured reflections. Four percent of the unique reflections measured initially were discarded because of partiality considerations, and 1% were excluded because of the conservative sigma-based cut.

Structure determination

The structure was solved by molecular replacement. Initial estimates of the phases for the P3/Sabin data were obtained by positioning a partially refined P1/Mahoney model in the P3/Sabin unit cell so that three of the particle 2-fold axes were coincident with the principal axes of the crystal, as required by the space group and by packing considerations. To refine these phases, the constraints which are imposed by noncrystallographic symmetry were applied by a modification of the iterative method of Bricogne (1974, 1976), using programs developed for a Convex C1 mini-supercomputer with a large (128 Mbyte) physical memory (D.J.Filman and J.M.Hogle, in preparation). The use of nonlinear interpolation [which allows maps to be sampled on a coarser grid without increasing interpolation error (Hogle *et al.*, 1986a)] makes it possible to hold the entire electron density map in memory, and improves the efficiency of the phase refinement considerably.

Model building and refinement

A complete atomic model, consistent with the known capsid sequence of P3/Sabin (Stanway *et al.*, 1983; Toyoda *et al.*, 1984) was built to fit the

averaged electron density map using the graphics program FRODO (Jones, 1985). The model was refined by alternating the application of noncrystallographic symmetry constraints, interactive model rebuilding and stereochemically constrained pseudo-real space refinement (D.J.Filman and J.M.Hogle, in preparation). The pseudo-real space procedure refines the atomic parameters by optimizing the agreement between resolution-scaled complex-valued transforms of the averaged and calculated electron densities, each evaluated over an arbitrary volume sufficient to enclose one protomer. An identical strategy has been used to refine the structure of P1/Mahoney.

Acknowledgements

We thank T.Critchlow for excellent technical assistance and M.Graber for assistance in preparation of the manuscript. Ribbon diagrams in Figure 1 were drawn by E.Getzoff. Space-filling representations were calculated using software by Connolly (1985). This work was supported by NIH grants AI20566 and GM38794 to J.M.H., by AI22627 to M.C. and by the World Health Organization. This is publication no. 5403-MB of the Research Institute of Scripps Clinic.

References

Abad-Zapatero,A., Abdel-Meguid,S.S., Johnson,J.E., Leslie,A.G.W., Rayment,I., Rossmann,M.G., Suck,D. and Tsukihara,T. (1980) *Nature*, **286**, 33–39.

Arnold,E. and Rossmann,M.G. (1988) *Acta Crystallogr.*, **A44**, 270–282.

Badger,J., Minor,I., Kremer,M.J., Olivera,M.A., Smith,T.J., Griffith,J.P., Guerin,D.M.A., Krishnaswamy,S., Luo,M., Rossmann,M.G., McKinlay,M.A., Diana,G.D., Dutko,F.J., Fancher,M., Rueckert,R.R. and Heinz,B.A. (1988) *Proc. Natl. Acad. Sci. USA*, **85**, 3304–3308.

Baron,M. and Baltimore,D. (1982) *Cell*, **28**, 395–404.

Bricogne,G. (1974) *Acta Crystallogr.*, **A30**, 395–405.

Bricogne,G. (1976) *Acta Crystallogr.*, **A32**, 832–847.

Burke,K.L., Dunn,G., Ferguson,M., Minor,P.D. and Almond,J.W. (1988) *Nature*, **332**, 81–82.

Chothia,C. and Lesk,A.M. (1987) *J. Mol. Biol.*, **196**, 901–917.

Chothia,C., Lesk,A.M., Levitt,M., Amit,A.G., Mariuzza,R.A., Phillips,S.E.V. and Poljak,R.J. (1986) *Science*, **233**, 755–758.

Chow,M., Newman,J., Filman,D.J., Hogle,J.M., Rowlands,D. and Brown,F. (1987) *Nature*, **327**, 482–486.

Connolly,M.L. (1985) *J. Mol. Graph.*, **3**, 19.

Diamond,D.C., Jameson,B.A., Bonin,J., Kohara,M., Abe,S., Itoh,H., Komatsu,T., Arita,M., Kuge,S., Nomoto,A., Osterhaus,A.D.M.E., Crainic,R. and Wimmer,E. (1985) *Science*, **229**, 1090–1093.

Fricks,C.E. (1988) PhD Thesis, University of California, San Diego.

Golden,J. and Harrison,S.C. (1982) *Biochemistry, (Wash.)*, **21**, 3862–3866.

Harrison,S.C., Olson,A.J., Schutt,C.E., Winkler,F.K. and Bricogne,G. (1978) *Nature*, **317**, 368–373.

Hogle,J.M., Chow,M. and Filman,D.J. (1985) *Science*, **229**, 1358–1365.

Hogle,J.M., Chow,M. and Filman,D.J. (1986a) In Moras,D., Drenth,J., Strandberg,B., Suck,D. and Wilson,K. (eds), *Crystallography in Molecular Biology*. Plenum Publishing Corp., New York, pp. 281–292.

Hogle,J.M., Maeda,A. and Harrison,S.C. (1986b) *J. Mol. Biol.*, **191**, 625–638.

Hosur,M.V., Schmidt,T., Tucker,R.C., Johnson,J.E., Gallagher,T.M., Selling,B.H. and Ruecker,R.R. (1988) *Proteins*, **2**, 167–176.

Icenogle,J.P., Minor,P.D., Ferguson,M. and Hogle,J.M. (1986) *J. Virol.*, **60**, 297–301.

Jones,T.A. (1985) *Methods Enzymol.*, **115**, 157–171.

Liljas,L., Unge,T., Jones,T.A., Fridborg,K., Lovgren,S., Skoglund,U. and Strandberg,B. (1982) *J. Mol. Biol.*, **159**, 93–108.

Luo,M., Vriend,G., Kamer,G., Minor,I., Arnold,E., Rossmann,M.G., Boege,U., Scraba,D.G., Duke,G.M. and Palmenberg,A.C. (1987) *Science*, **235**, 182–191.

McSharry,J.J., Caliguiri,L.A. and Eggers,H.J. (1979) *Virology*, **97**, 307–315.

Martin,A., Wychowski,C., Couderc,T., Crainic,R., Hogle,J.M. and Girard,M. (1988) *EMBO J.*, **7**, 2839–2847.

Minor,P.D., Schild,G.C., Bootman,J., Evans,D.M.A., Ferguson,M., Reeve,P., Spitz,M., Stanway,G., Cann,A.J., Hauptmann,R., Clarke,L.D., Mountford,R.C. and Almond,J.W. (1983) *Nature*, **301**, 674–679.

Minor,P.D., Evans,D.M.A., Ferguson,M., Schild,G.C., Westrop,G. and Almond,J.W. (1985) *J. Gen. Virol.*, **65**, 1159–1165.

Minor,P.D., Ferguson,M., Evans,D.M.A. and Icenogle,J.P. (1986) *J. Virol.*, **67**, 1283–1291.

Minor,P.D., Ferguson,M., Phillips,A., McGrath,D.I., Huovilainen,A. and Hovi,T. (1987) *J. Gen. Virol.*, **68**, 1857–1865.

Minor,P.D., Dunn,G., Evans,D.M.A., Magrath,D.I., John,A., Howlett,J., Phillips,A., Westrop,G., Wareham,K., Almond,J.W. and Hogle,J.M. (1989) *J. Gen. Virol.*, in press.

Murray,M.G., Bradley,J., Yang,X.-F., Wimmer,E., Moss,E.G. and Racaniello,V.R. (1988a) *Science*, **241**, 213–215.

Murray,M.G., Kuhn,R.J., Arita,M., Kawamura,N., Nomoto,A. and Wimmer,E. (1988b) *Proc. Natl. Acad. Sci. USA*, **85**, 3203–3207.

Page,G.S., Mosser,A.G., Hogle,J.M., Filman,D.J., Rueckert,R.R. and Chow,M. (1988) *J. Virol.*, **62**, 1781–1794.

Robinson,I.K. and Harrison,S.C. (1982) *Nature*, **297**, 563–568.

Rossmann,M.G., Arnold,E., Erickson,J.W., Frankenberger,E.A., Griffith,J.P., Hecht,H.-J., Johnson,J.E., Kamer,G., Luo,M., Mosser,A.G., Rueckert,R.R., Sherry,B. and Vriend,G. (1985) *Nature*, **317**, 145–153.

Rueckert,R.R. (1985) In Fields,B. (ed.), *Virology*. Raven, New York, pp. 705–738.

Smith,T.J., Kremer,M.J., Luo,M., Vriend,G., Arnold,E., Kamer,G., Rossmann,M.G., McKinlay,M.A., Diana,G.D. and Otto,M.J. (1986) *Science*, **233**, 1286–1293.

Stanway,G., Cann,A.J., Hauptman,R., Hughes,P., Clarke,L.D., Mountford,R.C., Minor,P.D., Schild,G.C. and Almond,J.W. (1983) *Nucleic Acids Res.*, **11**, 5629–5643.

Stauffacher,C., Usha,R., Harrington,M., Schmidt,T., Hosur,M.V. and Johnson,J.E. (1987) In Moras,D., Drenth,J., Strandberg,B., Suck,D. and Wilson,K. (eds), *Crystallography in Molecular Biology*. Plenum Publishing Corp. New York, pp. 293–308.

Toyoda,H., Kohara,M., Kataoka,Y., Suganuma,T., Omata,T., Imura,N. and Nomoto,A. (1984) *J. Mol. Biol.*, **174**, 561–585.

Westrop,G.D., Evans,D.M.A., Minor,P.D., Magrath,D., Schild,G.C. and Almond,J.W. (1986) In Rowlands,D.J., Mahy,B.W.J. and Mayo,M. (eds), *The Molecular Biology of the Positive Strand RNA Viruses*. Academic Press, London, pp. 53–60.

Winkler,F.K., Schutt,C.E. and Harrison,S.C. (1979) *Acta Crystallogr.*, **35**, 901–911.

Received on January 11, 1989

Note added in proof

Since the time of submission of this manuscript the structure of foot-and-mouth disease virus has been reported. The reference is Acharya,R., Fry,E., Stuart,D., Fox,G., Rowlands,D. and Brown,F. (1989) *Nature*, **337**, 709–716.